Back-illuminated Si photocathode

a combined experimental and theoretical study for photocatalytic hydrogen evolution

Bae, Dowon; Pedersen, Thomas; Seger, Brian; Malizia, Mauro; Kuznetsov, Andrej ; Hansen, Ole; Chorkendorff, Ib; Vesborg, Peter Christian Kjærgaard

Published in:
Energy & Environmental Science

Link to article, DOI:
10.1039/c4ee03723e

Publication date:
2015

Document Version
Publisher's PDF, also known as Version of record

Energy & Environmental Science

PAPER

View Article Online
View Journal

Cite this: DOI: 10.1039/c4ee03723e

Back-illuminated Si photocathode: a combined experimental and theoretical study for photocatalytic hydrogen evolution†

Dowon Bae,[a] Thomas Pedersen,[b] Brian Seger,[a] Mauro Malizia,[a] Andrej Kuznetsov,[c] Ole Hansen,[b] Ib Chorkendorff[a] and Peter C. K. Vesborg*[a]

Received 26th November 2014
Accepted 11th December 2014

DOI: 10.1039/c4ee03723e

www.rsc.org/ees

Si is an excellent absorber material for use in 2-photon photoelectrochemical hydrogen production. So far nearly all studies of silicon photoelectrodes have employed frontal illumination despite the fact that in most water-splitting 2-photon device concepts the silicon is the "bottom" cell in the tandem stack and therefore illuminated from the back with respect to the electrolyte. In the present work, we investigate back-illuminated Si photoelectrodes experimentally, as well as by modelling, the dependence of induced photocurrent on various parameters, such as carrier diffusion length (L_e) and surface recombination velocity (v_s) to quantify their relative importance. A bifacial light absorbing structure (p^+pn^+ Si) is tested under back-illumination conditions which mimic the actual working environment in a tandem water splitting device. The thickness of the absorbing Si layer is varied from 30 to 350 μm to assess the impact of the diffusion length/thickness ratio (L_e/L) on photocatalytic performance. It is shown how the induced photocurrent (J_L) of a back-illuminated sample increases as wafer thickness decreases. Compared to the 350 μm thick sample, a thinned 50 μm thick sample shows a 2.7-fold increase in J_L, and consequently also a higher open circuit voltage. An analytical model is developed to quantify how the relative L_e/L-ratio affects the maximum J_L under back-illumination, and the result agrees well with experimental results. J_L increases with the L_e/L-ratio only up to a certain point, beyond which the surface recombination velocity becomes the dominant loss mechanism. This implies that further efforts should to be focused on reduction of surface recombination. The present study is the first experimental demonstration of a Si wafer based photocathode under back-illumination. Moreover, the comparative experimental and theoretical treatment also highlights which photoabsorber properties merit the most attention in the further development towards full tandem water splitting devices.

1. Introduction

The development of semiconductor photocatalytic water splitting devices has attracted recent interest[1–5] because the direct conversion of solar energy into hydrogen is an attractive route to produce a clean chemical fuel.[2,6,7]

In order to be competitive with fossil fuels, artificial photosynthesis must be efficient and cheap. The overall process consists of two parts: (i) light absorption resulting in charge carrier generation and (ii) the utilization of excited photo carriers to drive catalytic reactions at the surface. It is thus essential to harvest a large fraction of the solar spectrum while ensuring efficient charge separation. Dual-absorber systems (sometimes called Z-scheme[8]), represent an efficient way to achieve wide spectral coverage using two semiconductors of different band gaps (E_g) as shown in Fig. 1. Effectively, the dual-absorber system works by series-connecting the high bandgap- and low bandgap-cells enabling a higher total voltage at the expense of current density.

In the case where silicon is used as the low-gap absorber (and as a photocathode in a dual-absorber arrangement) the flat-band potential of p-type silicon places severe restrictions on the voltage in an aqueous electrolyte.[9] However, by replacing the semiconductor–liquid junction with a pn^+-junction at the surface the flat-band limitation is mitigated. Such pn^+-Si electrodes have shown efficient electron–hole pair separation and increased open circuit voltage along with a higher current density[3,4,10,11] compared to p-Si electrodes.[9,12] In our previous

[a]Center for Individual Nanoparticle Functionality, Department of Physics, Technical University of Denmark, 2800 Kgs. Lyngby, Denmark. E-mail: Peter.Vesborg@fysik.dtu.dk; Fax: +45 4593 2399; Tel: +45 4525 3276

[b]Department of Micro- and Nanotechnology, Technical University of Denmark, 2800 Kgs. Lyngby, Denmark

[c]Centre for Materials Science and Nanotechnology, Department of Physics, University of Oslo, 0316 Oslo, Norway

† Electronic supplementary information (ESI) available: Supplementary information accompanies this paper including supplementary Fig. S1–S8; mathematical derivation procedure for analytical modelling; detail sample fabrication and equipment information for the experiments. See DOI: 10.1039/c4ee03723e

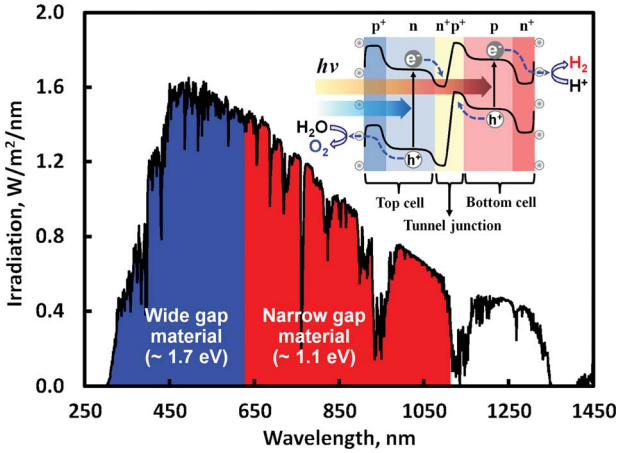

Fig. 1 Solar spectrum (AM 1.5G) coverage by dual absorbers based on a Z-scheme, and schematic of a device in a tandem design composed of dual pn-junctions, co-catalysts for oxygen and hydrogen evolution and recombination layer (tunnel junction) (inset). The top cell is formed in a wide band gap material and bottom cell in a narrow band gap material. The inset of this figure illustrates the carrier transfer along the band alignment under incident light. The short wavelength part of the light spectrum is absorbed by the top cell to oxidize water, while the longer wavelengths are absorbed by the bottom cell to produce H_2 gas.

work[10,11] it was found that pn^+-Si photocathodes with TiO_2 as a protection layer showed an open circuit voltage (V_{oc}) $\geq$ 0.5 V for the Hydrogen Evolution Reaction (HER). These electrodes also showed a maximum photocurrent (J_L) of 23 mA cm^{-2} under frontal illumination using the red spectrum shown in Fig. 1. This non-standard "red light only" illumination serves to simulate a real dual-absorber system where the blue light has been absorbed by the overlying (top) photoelectrode. In that case, 23 mA cm^{-2} corresponds to an Incident Photon to Current Efficiency (IPCE) of nearly 90%, while p-Si photocathodes (without the n^+ layer, but otherwise similar) showed V_{oc} of just 0.05 V with J_L of 17 mA cm^{-2} (IPCE of 61%).[9]

To date, various dual absorber water splitting devices have been demonstrated experimentally such as pn-$GaInP_2$/pn-GaAs,[13] pnp-$GaInP_2$/pn-GaAs.[14] These high-efficiency devices, however, are currently too expensive for large-scale applications. It seems that these materials also have severe scalability issues because Ga and In are elements which are by-products (of aluminum and zinc, respectively) and ultimately price-inelastic.[15] Various approaches have been demonstrated to substitute these high-cost materials with earth-abundant materials. A Si photocathode coupled to a metal oxide photoanode is one example.[16–18] However, the modest photocurrent density level of such structures ($J_{L,max} \approx$ 0.4 mA cm^{-2})[17] result in a low efficiency for water splitting. Nevertheless, progress is being made using oxides of lower band gap. A respectable state-of-the-art 3.6% solar-to-hydrogen (STH) efficiency tandem water splitting device based on a doped $BiVO_4$ photoanode in combination with single junction a-Si solar cell was recently demonstrated.[19] Despite recent progress,[3,20] developing a relatively simple dual absorber tandem structure is still an unsolved engineering challenge.

Using silicon as the bottom cell (*i.e.* under back-illumination – where light is incident from the "dry" side of the photoelectrode), a series of experiments showed that the photocurrent of a Si bottom cell was limited. The reason is that under back-illumination the electrode–electrolyte interface, which is the electron drain, is on the opposite side with respect to the incident light and since the wafer thickness is larger than the carrier diffusion length most electrons are lost to recombination near the back surface.[21,22] This problem of opposed light absorption and electrochemistry under back-illumination thus dictates a different approach to maximize the charge carrier utilization.

In this work we evaluate the experimental and theoretical maximum photocurrent ($J_{L,max}$) limit from the Si based photoelectrochemistry (PEC) system for hydrogen production under the back side illumination. The main focus is on maximum charge utilization of the Si photocathode under the assumption that it is used as a bottom cell in a tandem water splitting device. First we conducted experiments by using Czochralski (CZ) Si based cells with a pn-junction at the electrode/electrolyte interface side (type I configuration,[23] see Fig. S1a in ESI†), but varying the thickness to quantify the effect of the L_e/L-ratio on current–voltage (J–V) performance. We employed a light-permeable Al/p^+ charge collection backside layer, which allows illumination from the side opposing the solid/liquid interface while minimizing series resistance. A "buried junction" design (type II configuration,[23] see Fig. S1b in ESI†), whose pn^+-junction is on the illuminated side, can collect charge more efficiently. But the buried junction design requires a very highly doped layer (p^+) near the electrode–electrolyte interface to form an ultrathin space-charge region which allows electron tunnelling through the interface from the n-type bulk silicon to the electrocatalyst. Without such a layer the charge separation becomes very inefficient.[24] A key benefit of the type I structure is its ability to reduce the recombination loss of charge carriers by moving the pn-junction to opposite side with respect to the incident light since the presence of dopants increase local bulk recombination which can lead to reduced voltage loss.[25,26] Many state-of-art photovoltaic (PV) devices employ the same principle to enhance the blue-light response of the cells.[26,27] In addition, a shallow doped pn^+-junction formed at electrode–electrolyte interface provides band bending in the silicon independent of the electrolyte. On the other hand – moving the pn junction to the shadow-side of the device requires excellent surface passivation of the light incident side, as we shall see. Most devices in the literature are of a type I configuration, whereas a type II configuration has been demonstrated successfully by using multi-junction III–V [13-14] and by using a-Si PV devices.[19] In addition, we discuss a simplified model of the Si-based cell with the same cross-sectional structure as the aforementioned cell for the experiments to guide the choice of substrate properties: Surface recombination velocity (v_s), diffusion length (L_e) and thickness (L); for HER at maximum current density. The theoretical charge generation and collection models for the analytical calculation are discussed for this case, and finally, we compared the experimental results with the model-based calculation results verify the validity of the model.

2. Methods

2.1. Sample fabrication

CZ-Si based photocathodes of type I are fabricated with different wafer thickness in order to vary the L_e/L ratio (L = 30–350 μm) on otherwise similar electrodes. The thickness of the Si was varied by sample thinning (using photolithography and wet etching) of p-type Si substrates. Schematic drawings of samples used in this work are shown in Fig. 2 and S2a in ESI.† The shallow pn^+-junction was produced in p-type (100) Si wafers (Topsil, 1–20 ohm cm, boron-doped, acceptor density $N_A \approx 5 \times 10^{19}$ cm^{-3}) by thin n^+ doping using phosphorous ion implantation at 36 keV with a dose of 3×10^{15} cm^{-2} (donor density N_D of approximately 1×10^{20} cm^{-3}), which is expected to form a depletion width of 640 nm (described in detail in ESI†). As shown in our previous work,[10] this n^+ doping screens the band-bending in the silicon from the electrolyte, which allows for increased photovoltage.[3] As shown in Fig. 2c, the electron–hole pairs are separated by a built-in electric field which the pn^+ junction provides. The electrons are then transferred to the solid/liquid interface though the conduction band of TiO_2 using Mott-Schottky analysis (detail calculations are shown in ESI†). A mesa-isolated pn^+-Si structure with height of 3 μm is formed at the front side by photolithography and dry etching (Here, we used SF_6, O_2 and C_4F_8 gases in a Pegasus DRIE system from SPTS Technologies). The back side of the same samples were also doped with a thin p^+ doping using ion implantation of boron at 100 keV with a dose of 5×10^{16} cm^{-2} ($N_A \approx 1 \times 10^{20}$ cm^{-3}). A metallic charge collecting layer was deposited at room temperature by e-beam evaporation of Al. The Al layer was masked to create a circular hole over the active area in order to allow light transmission to the silicon. The resulting active area was precisely measured by image analysis using ImageJ 1.46r after the experiments. The p^+ doped layer in this device reduces overall series resistance by providing parallel path ways for holes to reach the Al charge collecting layer. Furthermore in actual tandem device operation condition it can also act as a part of the recombination layer (tunnel junction) for the injected holes from photocathode and the electrons from photoanode. Consequentially, the sample can be stated as a 'ready-made bottom cell' for tandem water splitting devices. Samples prepared without the p^+ doped layer are used to quantify the importance of the p^+ sheet-conducting layer (Fig. S5 in ESI†). In order to prevent the Si surface from photo-corrosion during the photo-electrochemical measurements, a Ti/TiO_2 (5/100 nm) protection layer was sputtered on the n^+ doped side (electrolyte side) of samples using previously published methods.[10,28] In case of TiO_2, Ti was reactively sputtered in an oxygen background. Prior to sputter deposition all wafers were dipped in buffered HF for 30 s, rinsed in Millipore water, dried and were then immediately placed in the sputter chamber to prevent the Si surface from deactivation by native oxide formation. All samples were cleaned with "piranha" solution (3 : 1 H_2SO_4 (96%) : H_2O_2 (30%)), washed with ultrapure water (18 MΩ cm) and dried before having 250 ng (Pt basis) of a dinitrosulphatoplatinate solution (Johnson Matthey) drop-cast on them. Pt was used as a co-catalyst in order to achieve high catalytic activity for HER. The thickness of the wafers was controlled using photolithographically thinned p-type Si substrates to keep the L_e value the same for all samples. Finally, they were coated with Teflon tape with a hole punched out yielding an active area of approximately 0.2 cm^2. This number was also precisely measured by optical image analysis after the experiments. In addition, the back side of the samples was covered with 50 μm thick quartz glass to protect back side from direct contact with the electrolyte. The quartz glass was mounted directly onto the Al layer using epoxy.

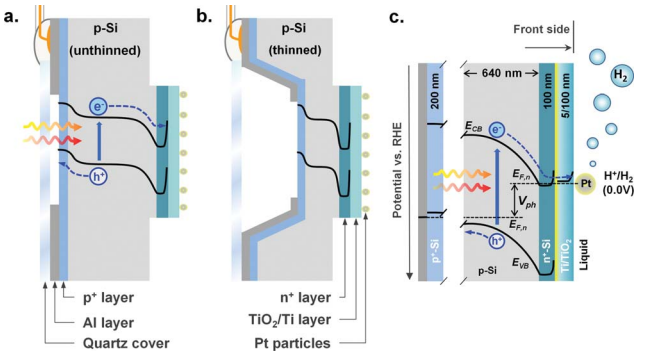

Fig. 2 Schematic cross section of the unthinned (a) and thinned device (b) used for photocatalytic activity (HER) experiments. The light is incident from the back side and HER occurs on the front side. In real device testing the back side of sample was protected by Quartz glass cover with epoxy to prevent corrosion in acidic electrolyte of the Cu-wire for electrical connection (covered with glue). Schematic energy diagram (c) of the illuminated sample in equilibrium with H^+/H_2 reaction is also shown. Detail calculation of energy diagram can be found in ESI (also in Fig. S3).†

2.2. Characterization

A 1000 W xenon lamp (Oriel) was used with a 635 nm cut-off filter and an AM 1.5 filter to simulate the red part of the solar spectrum. The light intensity reaching the sample was measured *via* a spectrophotometer (International Light Technologies Inc, RPS 900-R), and the light intensity was adjusted to match that of the total light intensity of red light in the AM 1.5G solar spectrum (λ > 635 nm, 41.8 mW cm^{-2}). For electrochemical measurements a Bio-Logic VSP potentiostat was used using EC Lab software. All cyclic voltammetry (CV) experiments were done in a 3 electrode H-cell design with an aqueous 1 M $HClO_4$ (Aldrich 99.99%) electrolyte. For all CV's the electrodes were scanned at a sweep rate of 10 mV s^{-1}. A Pt mesh was used as a counter electrode and the reference was a saturated $Hg/HgSO_4$ electrode (VWR International). The solution was purged with H_2 gas 30 minutes prior to any experiment and during the entire duration of the experiment. To determine efficiency as a function of wavelength, incident photon to current efficiency (IPCE) measurements were employed. An Oriel 74100 monochromator was combined with the Xenon lamp mentioned above to give monochromatic light. IPCE measurements were carried out from 500 to 900 nm for a thinned sample with a thickness of 50 μm under both front side and back side

illumination. Wavelengths below 500 nm are irrelevant in this (bottom cell) study and excluded using a filter. In order to determine the photocurrent, the electrodes were tested at 0.0 V *vs.* RHE using the same set-up and conditions as the CV measurements. The evolved H_2 was detected by gas chromatography (GC; Hewlett Packard 5890 Series II with a thermal conductivity detector, Ar carrier gas), and this is described in detail in ESI.†

2.3. Analytical model calculation

The generation rate is the number of electron–hole pairs generated at each point in the device due to the absorption of photons.[29,30] Neglecting reflection, the amount of incident light which is absorbed by a material depends on the absorption coefficient $\alpha = \alpha(\lambda)$ (unit cm^{-1}) and the thickness of the absorber. Assuming that the absorption of photons directly causes the generation of an electron–hole pair, the spectral generation rate, G, in a thin slice of absorber is determined by finding the change in light intensity across this thin slice, and consequently the electron–hole generation rate at any point in the device can be defined as follows:

$$G = \alpha H_0 e^{-\alpha z} \quad (1)$$

where H_0 is spectral photon flux density at the surface (photons per s per unit-area per wavelength increment), and z is distance into the absorber. The overall amount of generated charge at a certain depth is described in theoretical study section (Section 3.2). The spectral photon flux density H_0 can be calculated from measured irradiance $P(\lambda)$ of the solar simulator as the ratio of irradiance to photon energy using the equation shown below:

$$H_0 = \frac{\lambda P(\lambda)}{hc} \quad (2)$$

where λ is wavelength, c is the speed of light in vacuum, and h is Plank's constant. In the case where the surface is not perfectly non-reflecting, the irradiance is corrected by measured reflectivity at each wavelength (Fig. S8 in ESI†). The charge collection probability as a function of depth, $C_P(z)$, was calculated under the assumption that there is no excess electron density at the junction boundary (*i.e.* $n_e = 0$) while at $z = 0$ the surface recombination velocity requires $dn_e/dz = Sn_e$, where $S = v_s/D$ is the normalized surface recombination velocity, and v_s is the surface recombination velocity and D is diffusivity of Si. The excess electron density in steady state is governed by the steady state continuity equation:

$$\frac{d^2 n_e}{dz^2} = \frac{n_e}{{L_e}^2} \quad (3)$$

where $L_e = (D\tau_e)^{1/2}$ is the minority carrier diffusion length, and τ_e is carrier lifetime. The collection probability $C_P(z)$ is the probability that an electron–hole pair generated at a certain depth, z, will be collected (separated) by the pn-junction and consequently contribute to the photocurrent. The behavior of $C_P(z)$ and accompanying photo generated current densities J_L will be discussed later in theoretical study section, and details of the mathematical derivation can be found in the ESI.†

3. Results and discussion

3.1. Experimental study

Since we wish to illuminate from the back, a shallow boron doped p^+ layer, which is formed between the Al back current collector and the p-Si substrate, is used as a hole transport layer. The (control) sample without p^+ doped layer has a very low J_L at 0 V *vs.* RHE due to a high series resistance (Fig. S6 in ESI†). Furthermore, this p^+ doped layer works as a part of tunnel junction in practical tandem device. This structure makes the overall series resistance of the device comparable to a conventional Si device with direct back contact, and It was estimated that a doping concentration of 10^{20} cm^{-3} (5×10^{16} at per cm^2 implanted at 100 keV) of boron could provide a sufficiently low sheet resistance to the Si surface,[31] and consequently an efficient carrier transport pathway. Thus, a boron doped p^+ transport layer made by ion implantation method was used in the rest of samples in this study (device structure: p^+pn^+-Si). The photoelectrochemical properties of the p^+pn^+-Si photocathodes with different thicknesses (L = 350, 50 and 30 μm) were compared by measuring cyclic voltammetry. H_2 could be visually observed bubbling off from the semiconductor/liquid interface as the current increased, and it was confirmed by GC measurement that hydrogen is produced with high Faradaic efficiency (Fig. S9 in ESI†). As shown in Fig. 3 the fill-factor and photocurrent of 350 μm thick p^+pn^+-Si under front illumination (black dot) was considerably enhanced compared to that of the

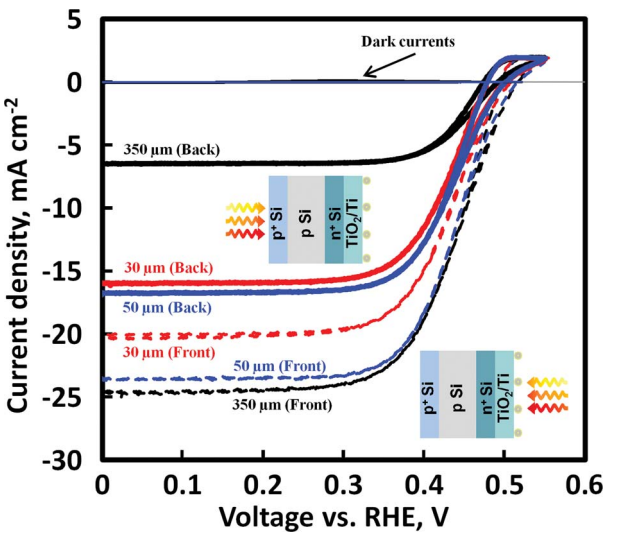

Fig. 3 CVs of Si photocathodes with unthinned design (black solid), *b* with 50 μm thick active area (blue solid) and 30 μm thick active area (red solid) under back-illumination, and under front-illumination (dotted lines). The total irradiance is 41.8 mW cm^{-2} (the light spectrum used in this figure can be found in Fig. 6). Assuming that L_e of all samples is same, this shows how L_e/L affects J_L of the device. The comparative study between back and front illumination indicates that the thinner the Si absorber is, the larger the ratio of J_L under back and front illumination is. However the $J_{L,max}$ of 30 μm thick sample with thinned design (red solid) is outperformed by the 50 μm thick sample indicating that absorption losses start to dominate the charge collection losses at around 50 μm thickness.

pn$^+$-Si in Fig. S6.† This demonstrates that adding the p$^+$ transport layer between the Al charge collector and p-Si significantly reduces the series resistance of the device. Under back-illumination the 350 μm thick p$^+$pn$^+$-Si sample showed a J_L of 6.2 mA cm^{-2}. This is significantly less current than the same sample generates under front-illumination. With the thinned design (Fig. 2b) a 50 μm Si slab increased the J_L to 17 mA cm^{-2} under back-illumination at the same light intensity. Since the only change between these samples is thickness, L, this can be considered a result of L_e/L ratio on overall charge to current conversion efficiency. As the *b* sample was thinned from its back side from 350 to 50 μm the L_e/L ratio should be seven fold larger. Since the diffusion length is the average distance that the excess carriers can cover before they recombine, increased L_e/L ratio should lead to improved J_L. Furthermore, V_{oc} of the thinned p$^+$pn$^+$-Si samples shifted slightly cathodic with increased J_L, and their slope improved under the back side illumination. This is likely due to the increased concentration of excited charge carriers. Indeed, the light induced open circuit voltage is given by the equation:

$$V_{oc} = \frac{nkT}{q}\ln\left(\frac{J_L}{J_0}+1\right) \quad (4)$$

where n is ideality factor of device, T is operating temperature, k is Boltzmann's constant, q is the electronic charge and J_0 is dark saturation current. Under the assumption that all samples have similar dark current and ideality factor, increased J_L leads to higher V_{oc}. In contrast, comparing unthinned sample with the thinned design (Fig. 2b) under front-illumination shows that thinning results in a lower J_L. The reason is that charge generation on average occurs closer to the pn-junction under front-illumination. As a result of the lower photocurrent density the V_{oc} is slightly lower under back-illumination than under front-illumination. This is probably due to a higher effective recombination velocity at the highly doped p$^+$ side than at the pn$^+$-side of the device.[32] Note also that the 30 μm thick Si sample with thinned design showed slightly lower current density (16.5 mA cm^{-2}) under back-illumination compared to the otherwise similar 50 μm thick sample even though it has a higher L_e/L ratio. This indicates a thickness of 30 μm is already below the critical thickness where the J_L starts to decrease (*i.e.* loss of photon absorption outweighs gain in $C_P(z)$).

Our spectrally resolved IPCE measurement results agree with this explanation. As shown in Fig. 4, the IPCE of a sample with thinned design increases gradually with wavelength under back-illumination, whereas it decreases gradually under the front-illumination. The absorption length δ_p is the distance into a material at which the light intensity drops by a factor of $1/e$ of its original intensity (*i.e.* the effective light penetration depth). Converting wavelength to δ_p in Si allows experimental estimation of $C_P(z)$ under the assumption of similar charge transfer and diffusion efficiency. As shown in the inset of Fig. 4, the IPCE was over 90% under front-illumination for photons, which are absorbed near the front side of the sample. Conversely, the same sample showed only approximately 50% IPCE under back-illumination. This shows that the pn$^+$-junction region separates charges better than the p$^+$p-region. The IPCE under back-illumination increases slowly from the short wavelength region and reaches a maximum at a wavelength near 900 nm. This behavior can be explained as follows: Photons with longer wavelengths penetrate deeper into the silicon. So under back-illumination electron–hole pairs generated from longer wavelength photons are therefore generated closer to the pn$^+$-junction boundary, whereas front illuminated case the photoabsorption depth as a function of wavelength is inverted, thus the IPCE shows the opposite behavior. This also can be supported by decrease of IPCE of thick samples under back illumination while IPCE under illumination from front side was almost invariable (Fig. S9 in ESI†).

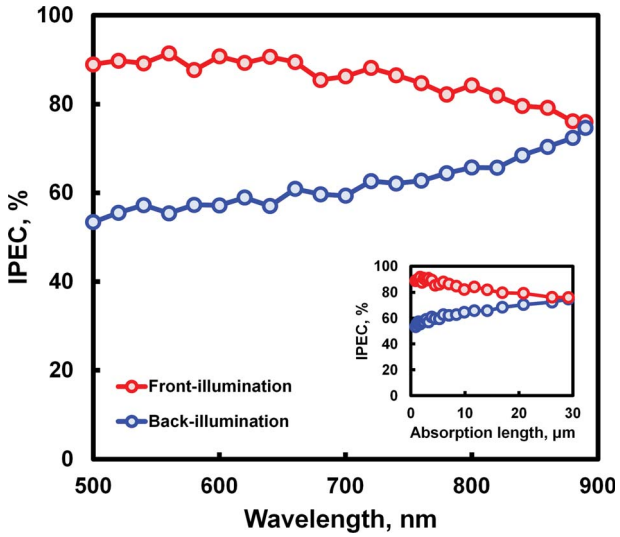

Fig. 4 IPCE measurement results under front and back-illumination using 50 μm thick thinned Si sample, and the inset is IPCE curve *versus* light absorption length (data is shown in Fig. S9 in ESI†) in Si.

Since the sample used for this IPCE measurement has a 50 μm thick Si slab, the IPCE response under both back and front illumination almost converge for wavelengths close to 900 nm.

3.2. Theoretical study

3.2.1. Ideal current density *vs.* effective thickness. Crystalline silicon has an indirect band gap (1.12 eV) and must therefore be thicker than most direct band gap light absorbers in order to have substantial optical absorption and electron–hole pair generation.[33] Fig. 5 shows, as an inset, the available photons *versus* wavelength in the reference solar spectrum (AM 1.5G).[34] The figure also shows the (red filtered) simulated solar spectrum used in this work where a Xe-lamp illumination is filtered using AM 1.5 and 635 nm-cut-off filters (*i.e.* $\lambda > 635$ nm to approximate the wavelengths and intensity would be received in a real tandem device).

The irradiance of solar light can be converted into a photogenerated electron–hole density (mA cm^{-2}) per unit wavelength for a Si-slab device of finite thickness. The resulting (integrated) current density is shown in Fig. 5 for both the AM 1.5G reference and for our simulated solar spectrum. If Si were to exhibit ideal

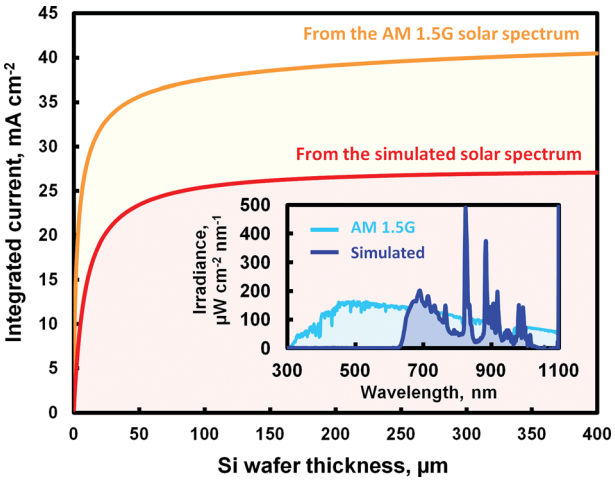

Fig. 5 Theoretical light-induced maximum current density in term of Si wafer thickness and the light spectrum of AM 1.5G and solar simulator with AM 1.5 and 635 nm-cut-off filters as an inset. The total irradiance of the simulated solar spectrum is 41.8 mW cm^{-2}, and for the standard AM 1.5G spectrum – 85.1 mW cm^{-2} with range from 250 to 1100 nm in wavelength.

behaviour of 100% internal quantum efficiency, *i.e.* zero recombination and infinite diffusion length, this electron–hole density ($J_{theo,max}$) would correspond to the measured photocurrent density. In the calculation of $J_{theo,max}$ the surface reflectance has been set to zero. The effect of surface reflectance will be addressed in detail later in this section. The current density due to photons which are absorbed during a single pass through the Si wafer with a certain thickness x can be theoretically calculated as follows:

$$J_{L,x} = \int_{\lambda_{min}}^{\lambda_g} q\frac{\lambda P(\lambda)}{hc}a(\lambda)\mathrm{d}\lambda \quad (5)$$

The integration limits are λ_g (the absorption edge of material), and λ_{min} (the shortest wavelength of the light) taken as 1100 nm and 250 nm in this work. The total irradiance of the (red filtered) simulated solar spectrum measured in this range was 41.8 mW cm^{-2}, which corresponds to the total light intensity of the standard AM 1.5G spectrum with range from 635 nm to 1100 nm. $a(\lambda)$ is the absorbance of the Si slab with a certain thickness, and can be approximated by Beer–Lambert law[35] (assuming that light only passes once through the cell and all light generated carriers are collected):

$$a(\lambda) = \frac{\alpha(\lambda)}{\ln 10}L \quad (6)$$

where L is Si thickness, and n is the index of refraction of the Si slab. The absorption coefficient $\alpha(\lambda)$ as a function of wavelength used in this work can be found in Fig. S7 in ESI.†

The absorbed light flux depends on the absorption length of the light in the silicon. As shown in Fig. 5, approximately 40 and 27 mA cm^{-2} of current density can be harvested in an ideal Si photoabsorber (if the Si is sufficiently thick), from AM 1.5G and (red filtered) simulated solar spectrum respectively. This figure also indicates that the integrated current density begins to saturate at thicknesses around 50 μm Si with a current density level of approximately 35.7 mA cm^{-2} and 23.5 mA cm^{-2}, under AM 1.5G and (red filtered) simulated solar spectrum respectively. This reveals that there is no need for using a thick wafer. In fact, a silicon back-electrode of just 15–25 μm thickness would be able to current match a 10 mA cm^{-2} – or even 15 mA cm^{-2} top electrode in a tandem device. However, as we shall see below, introduction of realistic losses recommends a somewhat thicker silicon absorber.

3.2.2. Charge collection model in a real Si device. In real Si devices finite charge recombination and charge diffusion lengths are major limiting factors reducing $J_{L,max}$. It is important to note that neither front nor back surface treatment for light trapping are used in experiments. Therefore we introduce the non-light trapping charge generation rate ($G(z)$), and the charge collection probability ($C_P(z)$) to quantify $J_{L,max}$ in real devices. We have introduced a simplified device model (Fig. 6) based on Si with a shallow pn^+-junction at the electrode–electrolyte interface. Schematic curves of $C_P(z)$ and $G(z)$ are shown in Fig. 7 to illustrate the principle. $C_P(z)$ depends on the distance that a light-generated carrier must travel compared to the diffusion length, L_e, and also on the surface properties of the device. If the carrier is generated further away from the junction than a diffusion length, ($z > L_e$), then the collection probability of this carrier is quite low. Similarly, if the carrier is generated closer to a region with high recombination (*e.g.* a non-passivated surface) than the junction, the carrier will recombine. Under, broad-band illumination most of the absorption (and electron–hole generation) takes place very close to the incident light surface (Fig. 6). Further absorption of low energy photons takes place throughout the bulk of the silicon, but the excitation density is small. However, the charge collection probability is highest near the pn^+-junction – *i.e.* the back side with respect to illumination. The dilemma is illustrated in Fig. 6.

The rate of light-generated carriers, G, as a function of depth z in Si can be theoretically calculated:

$$G(z) = \int_{\lambda_{min}}^{\lambda_g} \alpha(\lambda)H_0(\lambda)e^{(-\alpha(\lambda)z)}\mathrm{d}\lambda \quad (7)$$

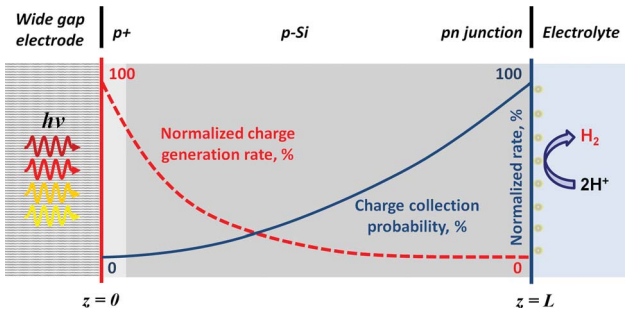

Fig. 6 Schematic of the simplified back-illuminated model device which is used in theoretical modelling. The normalized charge generation and charge collection probabilities in the device are also illustrated (not to scale) as a function of depth (z) inside the absorber with thickness L. It was assumed that optical properties of Si are homogeneous regardless of doping type.

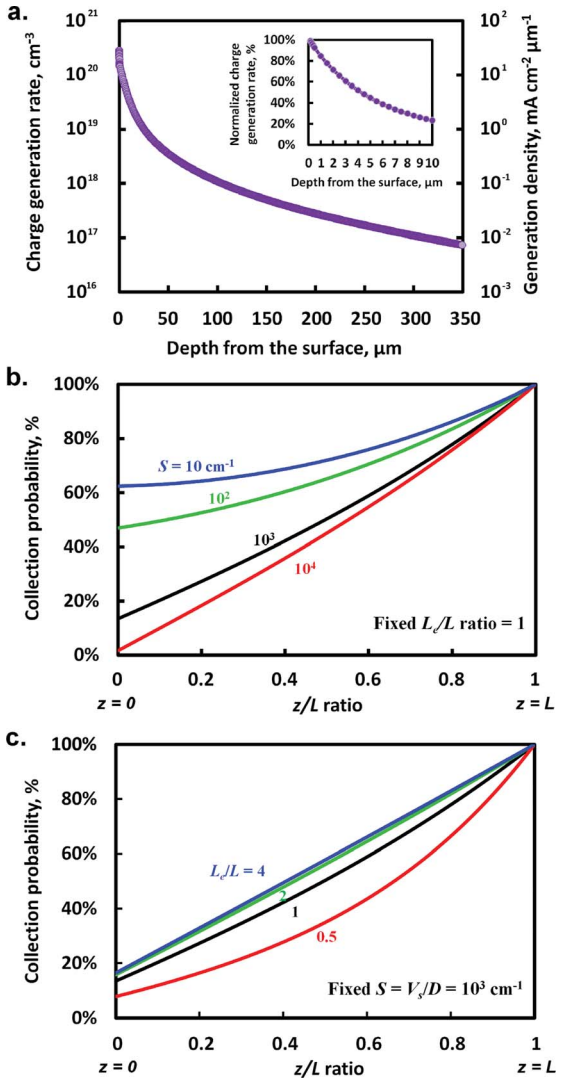

Fig. 7 Calculated charge generation induced by the light from the (red) simulated solar spectrum shown in Fig. 2a, calculated collection efficiency with various $S = V_s/D$ (b) and L_e/L (c) ratio. The normalized charge generation rate is ratio of charge generation rate to that at the surface ($z = 0$), where the value shows its maximum.

Fig. 8a shows behavior of $G(z)$ in terms of the depth from the light incident surface. An interesting point from Fig. 8a is that $G(z)$ drops below 50% of its initial value (*i.e.* at $z = 0$) just 5 μm from the surface. In fact, charge generation is almost zero at the junction boundary. This underscores the importance of charge collection probability ($C_P(z)$) since only collected charge become external photocurrent. The $C_P(z)$ as a function of depth, z, can be calculated from the equation shown below:

$$C_p(z) = \frac{1}{\cosh\frac{L-z}{L_e} + \sinh\frac{L-z}{L_e}\cdot\frac{\sinh\frac{z}{L_e} + SL_e\cosh\frac{z}{L_e}}{\cosh\frac{z}{L_e} + SL_e\sinh\frac{z}{L_e}}} \quad (8)$$

where S is the normalized surface recombination velocity (surface recombination velocity/diffusivity, $S = v_s/D$) and L, and L_e are the same as their previous definitions. eqn (8) was derived from the ratio of the charge flux at the pn-junction boundary to the sum of the fluxes generated in bulk as described in detail in ESI.† As shown in Fig. 7b and c, as one moves away from the junction at $z = L$, the collection probability drops. $C_P(z)$ becomes quite low at the surface (at $z = 0$) where electron–hole generation is fastest. The impact of surface recombination velocity and diffusion length on collection probability is also illustrated by varying S (and L_e/L) in eqn (8). As shown in Fig. 7b, $C_P(z)$ increases with the L_e/L ratio, and begins to saturate from an approximate ratio of $L_e/L = 2$ with $C_P(z)$ below 20% at the surface. Likewise, $C_P(z)$ increases with decreasing S, but unlike the L_e/L ratio, $C_P(z)$ at the surface ($z = 0$) increases significantly as S value decreases. This indicates that increasing the diffusion length (L_e) increases the charge collection efficiency ($C_P(z)$) only up to a certain point. Beyond this point further increase of diffusion length of the Si (*i.e.* the bulk quality of the Si) has little benefit for charge collection since in that limit the total recombination is dominated by surface recombination. This behavior of $C_P(z)$, and consequently $J_{L,max}$ for different thicknesses is shown as a function of S and L_e in Fig. 8. The $J_{L,max}$ can be calculated from the equation shown below by multiplying $G(z)$ and $C_P(z)$ of the carriers:

$$J_{L,max} = q\int_0^L G(z)C_p(z)dz \quad (9)$$

As shown in each plot of Fig. 8, once L_e reaches a certain value comparable to the absorber thickness, surface recombination (S) starts to become more significant. As shown in Fig. 8a ($L = 15$ μm), the slopes of contour lines are relatively moderate in the short diffusion length region and the gap between the lines have been broadened. This indicates J_L in a real device will be less sensitive to device parameters, but the maximum current for 15 μm thick Si is limited below 17 mA cm^{-2} while a 30 μm thick Si (Fig. 8b) can reach above 20 mA cm^{-2}. The thinnest samples are limited by photons with long wavelength passing through the Si with little absorption. On the other hand, a 350 μm thick device (Fig. 8f) shows a J_L limited at approximately 10 mA cm^{-2} and even this value requires good surface passivation and a very high L_e level which only can be achieved by using quality material such as float zone (FZ) Si.

The reason is that charge collection probability with identical S and L_e decreases with increased Si thickness due to the decreased L_e/L ratio and the impact of this ratio increases significantly as thickness of Si increases as already shown in Fig. 7c. Clearly, the choice of thickness is strongly dependent on L_e and S and must be optimized with respect to cost. Considering that conventional solar cell grade CZ Si wafer shows L_e of 100–300 μm,[35] using Si with thickness around 50 μm seems an appropriate compromise. As shown in Fig. 8c, 50 μm thick Si shows peak values up to 20.2 mA cm^{-2} under the $\lambda > 635$ nm simulated spectrum. This is a high J_L value compared to the other thicknesses with identical S and L_e.

However, in order to compare to experimental results it is necessary to include the surface reflectance from the light incident side. Considering measured reflectance from the back

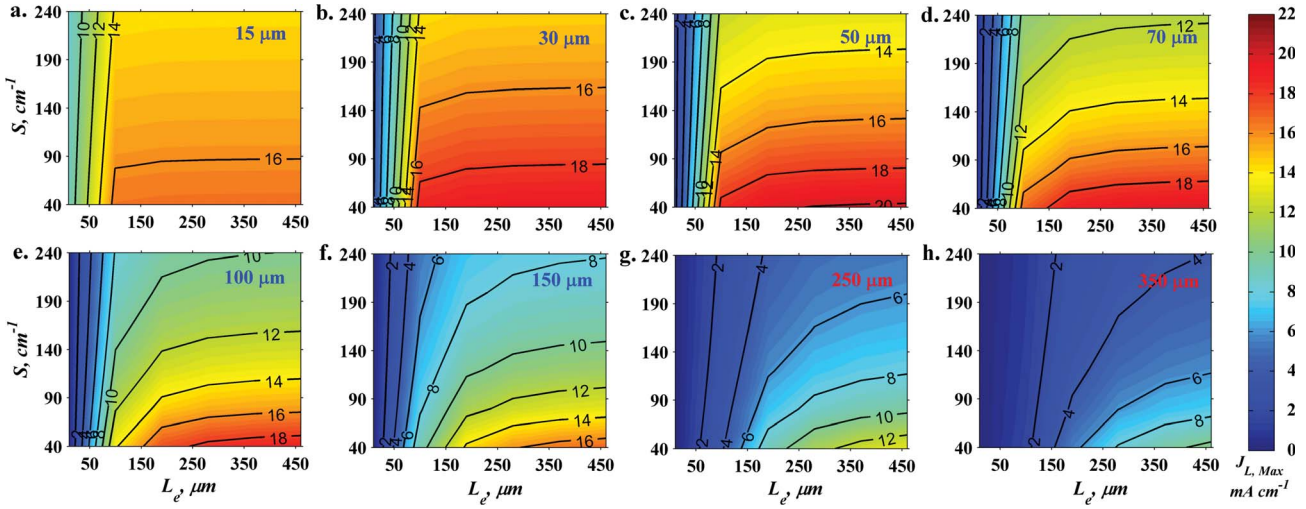

Fig. 8 Contour plots of theoretical maximum current density *versus* diffusion length and surface recombination rate for 15 μm thick (a), 30 μm thick (b), 50 μm thick (c), 70 μm thick (d), 100 μm thick (e), 150 μm thick (f), 250 μm thick (g), and 350 μm thick (h) bottom cell under the simulated bottom cell illumination (see Fig. 2). These plots illustrate impact of S and L_e on theoretical current density, and at the same time how these impacts change with Si thickness.

side of the device (solid blue curve in Fig. S11†), the theoretical maximum current with surface reflectance $J'_{L,\max}$ can be calculated. The result is reduced charge generation rate $G'(z)$ due to the surface reflectance. As shown in Fig. 10, it is observed that the overall current level is decreased by more than 15% for all three thicknesses due to the surface reflectance. Overlapping contour lines, which correspond to the experimental values with uncertainty, allows estimating approximate L_e and S values of the Si device used in this work (green colored area in Fig. 9d). It was found that a L_e of approximately 350 μm and S of 80 cm^{-1} best fit the experimental data. Assuming that Si has an electron diffusivity, $D \leq 36$ cm^2 s^{-1},[36] we estimate the surface recombination velocity, V_s, to be approximately 3×10^3 cm s^{-1} ($S = V_s/D$). This high value clearly indicates that there is room for improvement. Using these traced values one can determine the theoretical Absorbed Photon-to-Current Efficiency (APCE). For Pt, a material with fast HER kinetics, the yield of electron injection into the electrolyte is ~1, and therefore APCE can be obtained by dividing J_L by absorbed photon expressed as a current density (J_{abs}).[37] Details of the mathematical procedure can be found in the ESI.† It was determined that the APCE, which was calculated from the measured IPCE, was quite similar to $C_P(z)$ with L_e of 350 μm and S of 80 cm^{-1} (Fig. S12 in ESI†), indicating that the measured experimental behaviour agrees well with the model.

In Fig. 10, the calculated current density (using an empirical L_e and S extracted from Fig. 9) is shown as a function of thickness together with five experimentally measured values (Fig. S13 in ESI†). Calculated photocurrent density with enhanced L_e and S cases are also shown to point out how additional improvements can be made with further structural design modification. An important point is the impact of surface recombination velocity on $J'_{L,\max}$. According to the modeled data in Fig. 10, an improvement of S (dashed line) gives higher impact on $J_{L,\max}$ than an improvement in L_e. Case in point: $J_{L,\max}$ increased by 12% when S is reduced by 1/2, whereas a model of a device with 3× increased L_e (dot-dash line) shows only slight increase in current density with decreased thickness sensitivity. This analysis strongly suggests using (back) surface passivation – *e.g. via* application of a thermally grown SiO_2 layer[38] or an overlayer

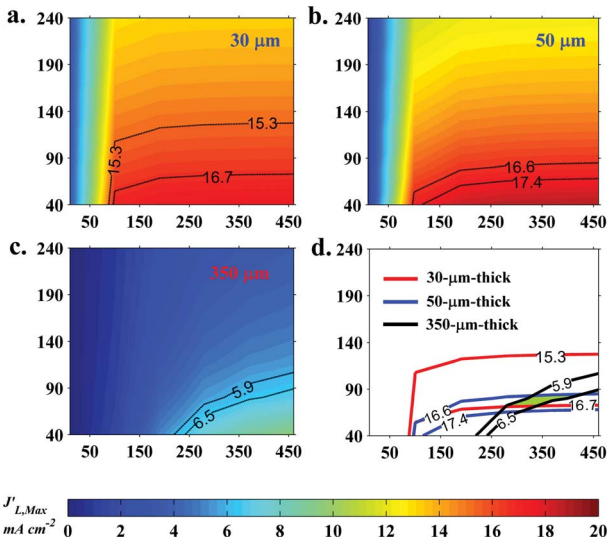

Fig. 9 Contour plot of theoretical maximum current density *versus* diffusion length and surface recombination rate under simulated illumination (Fig. 6) considering reflectance from the surface of the back side *versus* diffusion length and surface recombination rate for 30 μm thick (a), 50 μm thick (b), 350 μm thick (c). Overlapped contour lines (d) which correspond to the experimental uncertainty are also given to estimate diffusion length and surface recombination rate of the samples used for this work. Uncertainty ranges for each panel were derived from the uncertainty of the saturated current I_L and the active area measurement A, *i.e.* $I_L/A \pm (\Delta I_L + \Delta A)$.

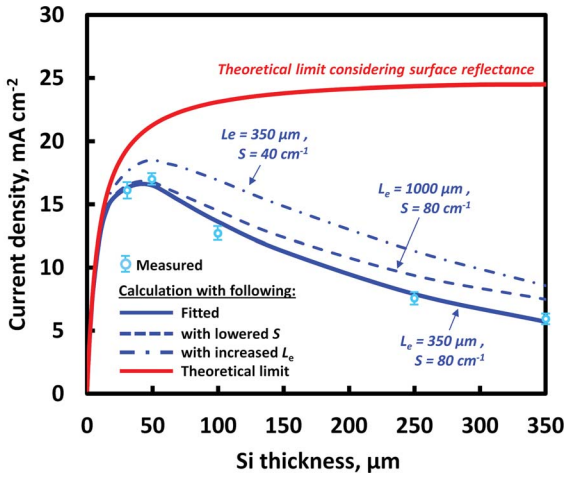

Fig. 10 Calculated theoretical limits of the current density: curve from the Si device with recombination rate and diffusion length value traced from the IPCE and modelling data ($L_e = 175$ μm; $S = 0.48$ cm^{-1}) (blue solid), and estimated behavior from the device with increased L_e and S (blue dots). Theoretical limit of an ideal Si device, *i.e.* $L_e = \infty$ and $S = 0$ (red curve) with surface reflectance is also given for comparison.

of ZnO or Al_2O_3 [39] – in order to reduce the surface recombination velocity. As described in Fig. S2,† the back side surface of the Si samples (the top surface in figure) is exposed to atmosphere, and thus one would expect there to be a native grown SiO_2 layer (~1 nm) of poor quality, which does not provide good surface passivation. Furthermore, since the back side of bottom cell must provide an Ohmic contact with the top cell in tandem designs the internal passivation layer should be conductive as well as transparent. This suggests that either a transparent conducting oxide (TCO) with locally opened-point contacts[40,41] or a design with a very thin dielectric passivation layer is attractive.[38,39] Amorphous Si (a-Si:H) with a TCO overlayer can be an excellent candidate as demonstrated by Panasonic HIT cell,[26] since a-Si:H has excellent passivation capability and enable good carrier transport. It should be noted that the conduction band position of the n-type TCO layer should be close to the valence band of p^+ Si surface,[42] since these layers should work as a tunnel junction in practical tandem device.

4. Conclusions

We have demonstrated, for the first time, a back-illuminated photocathode which is suited to work efficiently in a tandem PEC stack. Specifically we have shown that a photocathode with a p^+pn^+-Si – structure, whose pn-junction is formed at the solid/liquid side, can be used as a HER photoelectrode under back side (dry side) illumination which is similar to actual operational conditions in tandem water splitting devices. From an analytical calculation study, it was found that the balance between charge collection probability and light absorber thickness is an important design parameter to produce efficient back-illuminated devices. The photoelectrochemical investigation of p^+pn^+-Si with Si-thickness as parameter clearly demonstrates the impact of L_e/L ratio estimated from the above-mentioned theoretical results. A 50 μm thick thinned p^+pn^+-Si electrode showed a maximum J_L (17.0 mA cm^{-2}) under back-illumination, whereas a 350 μm thick sample, with a 7 times lower L_e/L ratio, showed only 6.1 mA cm^{-2}. In contrast, despite its enhanced L_e/L ratio, a 30 μm thick sample showed only slightly lower J_L due to its limited light absorption (loss of infrared photons). These results demonstrate how the charge collection limitation of a photocathode with its pn-junction at solid/liquid can be overcome. Importantly, the increased fill factor and increased V_{oc} of the thinned back-illuminated samples owe their success mostly to increased J_L, and such designs should lead to increased operational current density when coupled with a photoanode. Building on the experimental input, further modelling shows that surface recombination on the back side of the silicon is the dominant current loss mechanism. Therefore, the application of a conducting passivation layer, which allows transport of the carriers with minimum optical loss, seems one of the critical challenges to reduce the back side recombination rate and consequently enhance photocatalytic performance of practical Si-bottom cell.

Acknowledgements

This work was performed as a part of the Center for Individual Nanoparticle Functionality (CINF) which is funded by Danish National Research Foundation (DNRF54). Furthermore, most of sample fabrication work has been done using facilities in DTU Danchip.

Notes and references

1 N. S. Lewis and D. G. Nocera, Powering the planet: chemical challenges in solar energy utilization, *Proc. Natl. Acad. Sci. U. S. A.*, 2006, **103**, 15729–15735.
2 M. G. Walter, E. L. Warren, J. R. McKone, S. W. Boettcher, Q. Mi, E. A. Santori and N. S. Lewis, Solar water splitting cells, *Chem. Rev.*, 2010, **110**, 6446–6473.
3 S. W. Boettcher, E. L. Warren, M. C. Putnam, E. A. Santori, D. Turner-Evans, M. D. Kelzenberg, M. G. Walter, J. R. McKone, B. S. Brunschwig, H. A. Atwater and N. S. Lewis, Photoelectrochemical hydrogen evolution using Si microwire Arrays, *J. Am. Chem. Soc.*, 2011, **133**, 1216–1219.
4 M. Moriya, T. Minegishi, H. Kumagai, M. Katayama, J. Kubota and K. Domen, Stable hydrogen evolution from CdS-modified $CuGaSe_2$ photoelectrode under visible-light irradiation, *J. Am. Chem. Soc.*, 2013, **135**, 3733–3735.
5 C. G. Morales-Guio, S. D. Tilley, H. Vrubel, M. Grätzel and X. Hu, Hydrogen evolution from a copper(I) oxide photocathode coated with an amorphous molybdenum sulphide catalyst, *Nat. Commun.*, 2014, **5**, 3059.
6 S. Dahl and I. Chorkendorff, Solar-fuel generation: becoming practical?, *Nat. Mater.*, 2012, **11**, 100–101.
7 R. Schlögl, Chemistry's role in regenerative energy, *Angew. Chem., Int. Ed.*, 2011, **50**, 6424–6426.
8 A. J. Bard, Photoelectrochemistry and heterogeneous photocatalysis at semiconductors, *J. Photochem.*, 1979, **10**, 59–75.

9 Y. Hou, B. L. Abrams, P. C. K. Vesborg, M. E. Björketun, K. Herbst, L. Bech, A. M. Setti, C. D. Damsgaard, T. Pedersen, O. Hansen, J. Rossmeisl, S. Dahl, J. K. Nørskov and I. Chorkendorff, Bioinspiredco-catalysts bonded to a Silicon photocathode for solar Hydrogen evolution, *Nat. Mater.*, 2011, **10**, 434–438.

10 B. Seger, T. Pedersen, A. B. Laursen, P. C. K. Vesborg, O. Hansen and I. Chorkendorff, Using TiO_2 as a conductive protective layer for photocathodic H_2 evolution, *J. Am. Chem. Soc.*, 2013, **135**, 1057–1064.

11 B. Seger, A. B. Laursen, P. C. K. Vesborg, T. Pedersen, O. Hansen, S. Dahl and I. Chorkendorff, Hydrogen production using a molybdenum sulfide catalyst on a titanium-protected n+p-silicon photocathode, *Angew. Chem., Int. Ed.*, 2012, **51**, 9128–9131.

12 E. L. Warren, S. W. Boettcher, J. R. McKone and N. S. Lewis, Photoelectrochemical water splitting: silicon photocathodes for hydrogen evolution, *Proc. SPIE*, 2010, **7770**, 77701F.

13 B. O. Khaselev and J. A. Turner, A monolithic photovoltaic-photoelectrochemical device for hydrogen production *via* water splitting, *Science*, 1998, **280**, 425–427.

14 X. Gao, S. Kocha, A. J. Frank and J. A. Turner, Photoelectrochemical decomposition of water using modified monolithic tandem cells, *Int. J. Hydrogen Energy*, 1999, **24**, 319–325.

15 P. C. K. Vesborg and T. F. Jaramillo, Addressing the terawatt challenge: scalability in the supply of chemical elements for renewable energy, *RSC Adv.*, 2012, **2**, 7933–7947.

16 R. H. Coridan, M. Shaner, C. Wiggenhorn, B. S. Brunschwig and N. S. Lewis, Electrical and photoelectrochemical properties of WO_3/Si tandem photoelectrodes, *J. Phys. Chem. C*, 2013, **117**, 6949–6957.

17 M. R. Shaner, K. T. Fountaine, S. Ardo, R. H. Coridan, H. A. Atwater and N. S. Lewis, Photoelectrochemistryof core–shell tandem junction n-p^+-Si/WO_3 microwire array photoelectrodes, *Energy Environ. Sci.*, 2014, **7**, 779–790.

18 J. A. Turner, A nickel finish protects silicon photoanodes for water splitting, *Science*, 2013, **342**, 811–812.

19 F. F. Abdi, L. Han, A. H. M. Smets, M. Zeman, B. Dam and R. van de Krol, Efficient solar water splitting by enhanced charge separation in a bismuth vanadate-silicon tandem photoelectrode, *Nat. Commun.*, 2013, **4**, 2195.

20 J. Brillet, J.-H. Yum, M. Cornuz, T. Hisatomi, R. Solarska, J. Augustynski, M. Graetzel and K. Sivula, Highly efficient water splitting by a dual-absorber tandem cell, *Nat. Photonics*, 2012, **6**, 824–828.

21 N. Wyrsch, S. Dunand and C. Ballif, Bifacial a-Si:H solar cells: Origin of the asymmetry between front and back illumination, *Proceedings of NUMOS*, 2007, 289–295.

22 A. Kränzl, R. Kopecek, K. Peter and P. Fath, Bifacial solar cells on multi-crystalline silicon with boron BSF and open rear contact, *Conference Record of the 2006 IEEE 4th World Conference on Photovoltaic Energy Conversion*, 2006, vol. 1, pp. 968–971.

23 S. Hu, C. Xiang, S. Haussener, A. D. Berger and N. S. Lewis, An analysis of the optimal band gaps of light absorbers in integrated tandem photoelectrochemical water-splitting systems, *Energy Environ. Sci.*, 2013, **6**, 2984–2993.

24 J. J. H. Pijpers, M. T. Winkler, Y. Surendranath, T. Buonassisi and D. G. Nocera, Light-induced water oxidation at silicon electrodes functionalized with a cobalt oxygen-evolving catalyst, *Proc. Natl. Acad. Sci. U. S. A.*, 2011, **25**, 10056–10061.

25 D. L. Meier, H. P. Davis, R. A. Garcia, J. Salami, A. Rohatgi, A. Ebong and P. Doshi, Aluminum alloy back p–n junction dendritic web silicon solar cell, *Sol. Energy Mater. Sol. Cells*, 2001, **65**, 621–627.

26 Panasonic headquarter news,http://panasonic.co.jp/corp/news/official.data/data.dir/2014/04/en140410-4/en140410-4.html, accessed November 2014.

27 D. D. Smith, P. J. Cousins, A. Masad, A. Waldhauer, S. Westerberg, M. Defensor, R. Ilaw, T. Dennis, R. Daquin, N. Bergstrom, A. Leygo, Z. Xi, B. Meyers, B. Bourne, M. Shields and D. Rose, SunPower's Maxeon Gen III solar cell: High efficiency and energy yield, *Proc. 39th IEEE PVSC, IEEE*, New York, 2013, pp. 0908–0913.

28 Y. Lin, C. Battaglia, M. Boccard, M. Hettick, Z. Yu, C. Ballif, J. W. Ager and A. Javey, Amorphous Si thin film based photocathodes with high photovoltage for efficient hydrogen production, *Nano Lett.*, 2013, **13**, 5615–5618.

29 F. Y. R. El Faituri and A. Y. Darkwi, Computer simulation for current density in pn-Si solar cells, *Proceedings of the International Symposium on Solar Physics and Solar Eclipses*, Waw an Namus, 2006.

30 C. Hu and R. M. White, *Solar Cells: from basics to advanced systems*, ed. W. Stephen, McGraw-Hill college, New York, 1st edn, 1983, ch. 3.3, pp. 45–46.

31 W. R. Thurber, R. L. Mattis, Y. M. Liu and J. J. Filliben, Resistivity-dopant density relationship for boron-doped silicon, *J. Electrochem. Soc.*, 1980, **127**, 2291–2294.

32 A. F. Thomson and K. R. McIntosh, Light-enhanced surface passivation of TiO_2-coated silicon, *Prog. Photovoltaics*, 2012, **20**, 343–349.

33 P. Bosshard, W. Hermann, E. Hung, R. Hunt and A. J. Simon, An assessment of solar energy conversion technologies and research opportunities, *GCEP Energy Assessment Analysis*, Stanford University, 2006.

34 ASTM G173-03, Standard tables for reference solar spectral irradiances:direct normal and hemispherical on 37° tilted surface, 2012.

35 V. A. Milichko, A. I. Nechaev, V. A. Valtsifer, V. N. Strelnikov, Y. N. Kulchin and V. P. Dzyuba, Photo-induced electric polarizability of Fe_3O_4 nanoparticles in weak optical fields, *Nanoscale Res. Lett.*, 2013, **8**, 317–323.

36 D. L. Losee, Admittance spectroscopy of impurity levels in Schottky barriers, *J. Appl. Phys.*, 1975, **46**, 2204–2214.

37 T. W. Kim and K.-S. Choi, Nanoporous $BiVO_4$ photoanodes with dual-layer oxygen evolutioncatalysts for solar water splitting, *Science*, 2014, **343**, 990–994.

38 F. Feldmann, M. Simon, M. Bivour, C. Reichel, M. Hermle and S. W. Glunz, Carrier-selective contacts for Si solar cells, *Appl. Phys. Lett.*, 2014, **104**, 181105.

39 D. Garcia-Alonso, S. Smit, S. Bordihn and W. M. M. Kessel, Silicon passivation and tunneling contact formation by

atomic layer deposited Al_2O_3/ZnO stacks, *Semicond. Sci. Technol.*, 2013, **28**, 082002.

40 A. Goodrich, P. Hacke, Q. Wang, B. Sopori, R. Margolis, T. L. James and M. Woodhouse, A wafer-based monocrystalline silicon photovoltaics roadmap: Utilizing known technology improvement opportunities for further reductions in manufacturing costs, *Sol. Energy Mater. Sol. Cells*, 2013, **114**, 110–135.

41 J. Schmidt, M. Kerr and A. Cuevas, Surface passivation of silicon solar cells using plasma-enhanced chemical-vapour-deposited SiN films and thin thermal SiO_2/plasma SiN stacks, *Semicond. Sci. Technol.*, 2001, **16**, 164–170.

42 Y.-S. Lin, S.-Y. Lien, C.-C. Wang, C.-H. Hsu, C.-H. Yang, A. Nautiyal, D.-S. Wuu, P.-C. Tsai and S.-J. Lee, Optimization of recombination layer in the tunnel junction of amorphous silicon thin-film tandem solar cells, *Int. J. Photoenergy*, 2011, **2011**, 264709.